

# Dynamic structural response of DEMO divertor under electromagnetic loading

Kuo Zhang<sup>a,c</sup>, Nicolas Mantel<sup>b</sup>, Jeong-Ha You<sup>c</sup>

*a Karlsruhe Institute of Technology, Hermann-von-Helmholtz-Platz 1, 76344 Eggenstein-Leopoldshafen, Germany*

*b Culham Centre for Fusion Energy, Abingdon, Oxfordshire, OX14 3DB, Great Britain*

*c Max Planck Institute for Plasma Physics, Boltzmannstraße 2, 85748 Garching, Germany*

*\*Corresponding author: kuo.zhang@kit.edu*

The divertor of a tokamak-type fusion reactor is subject to the potential risk of accidental plasma disruptions. This fast transient event produces strong and brief electromagnetic (EM) excitation loads exerting in the divertor in form of volume forces and moments. Moreover, the transient nature of the impact loads could cause a substantial dynamic amplification of the Lorentz forces and moments due to the interaction between the (transient) resonance and mass inertia. This dynamic amplification effect must be considered in the structural design of the divertor in addition to the static loads. One pragmatic approach to do this is to apply the notion of dynamic amplification factor (DAF) as a kind of a force multiplier coefficient in order to reflect the dynamic effect in a static stress analysis. To this end, the dynamic amplification factor needs to be determined for the given geometry of the components and the typical application modes of relevant impact loads. The key objective of this dynamic analysis is to identify the natural frequencies (eigen-frequency) and the deformation modes. The dynamic effect on the stress intensity in the critical regions is also examined. This study presents a unique insight into the structural dynamics induced by a plasma disruption and delivers a very useful design parameter for the force component of the load, namely, dynamic amplification factor which allows a straightforward way of considering the resonance response in a static structural analysis.

*Keywords: dynamic amplification factor, fixation, static/dynamic response*

| Abbreviation | Definition                   |
|--------------|------------------------------|
| EM           | Electro-Magnetic             |
| FEM          | Finite Element Method        |
| MPH          | Material Properties Handbook |
| DAF          | Dynamic amplification        |
| IVT          | Inner vertical target        |

|     |                       |
|-----|-----------------------|
| OVT | Outer vertical target |
| RP  | Reflector plate       |
| VV  | Vacuum vessel         |

## 1. Introduction

Under the impact loads generated by strong and brief electromagnetic (EM) volume forces and moments [1, 2], the divertor of DEMO tokamak fusion reactor experiences dynamic resonance. Due to the interaction between the (transient) resonance and mass inertia in this dynamic loads, the consequent strain, stress, displacements, damage, etc. have been amplified comparing to the corresponding values with static loads.

In order to allow the monotonic damage assessment based on static analysis, a conservative dynamic amplification factor (DAF) is to be determined for Equation 1, Equation 2 and Equation 3.

In the static analysis, all loading are to be amplified by the DAF; while in the dynamic analysis where velocity and acceleration is included, original loading are applied and the effect of mass inertia is considered within the calculation. A DAF shall be chosen, so as to make the resultant strain/stress/displacement from the static analysis be equal to or larger than the corresponding values from the dynamic analysis. This is a pragmatic approach to consider the dynamic amplification effect in the structural design of the divertor in addition to the static loads.

Equation 1 
$$\varepsilon_{static}(F \times DAF) \geq \varepsilon_{dyn}(F)$$

Equation 2 
$$\sigma_{static}(F \times DAF) \geq \sigma_{dyn}(F)$$

The micro-strain adds up to macro-displacement:

Equation 3 
$$U(F \times DAF) \geq U(F)$$

This DAF shall depend on a sequence of influencing factors, including the eigen-frequency of the structure  $\omega_0$ , profiles of external loading, damping factors ( $\alpha$  &  $\beta$ ), etc. Since these input values of real divertor are currently difficult to be determined, it is valuable to initially build some simple structures, such as a bar, with simple loading profiles for a methodology for a conservative DAF.

Note that this methodology is different from the one in a traditional resonating system, since the external EM loading is not cyclic, but instead acts as an impact which happens only once.

This work started with the literature study to search for an analytical solution of DAF. Methodology study has been performed to evaluate whether the mathematical theory for general resonating system is applicable to the analysis of EM loading on divertor.

The energy of a vibrating structure is dissipated by various mechanisms, and the damping is a macro-scale manifestation of these dissipation[3]. Hence the damping factor of a structure is not a simple combination of

damping of single components. The damping factor can only be determined through testing on the actual structure in laboratory. According to [4], the factor is 4 % for welded steel or bolted steel with friction connection, which is applicable for global seismic analyses of the tokamak machine.

A model of DEMO divertor [5, 6] has been implemented into commercial finite element code ABAQUS [7]. To avoid too long time calculation and high cost on computing devices, a very detailed 3D model of DEMO divertor has been firstly simplified by deleting local details and keeping the dimension and stiffness of the whole structure.

Four groups of simulations have been performed with different setups of boundary conditions in ABAQUS under the concept of Parametric Digital Model Development [8] to evaluate the relationship between design parameters and CAD model parameters. After frequency analysis, displacements in static and dynamic analysis have been compared and the ratios between them have been calculated. The DAF for each group has been proposed, by comparing the displacements and stress states in the amplified static analysis to those in corresponding dynamic analysis.

## 2. Literature and methodology study for the determination of analytical DAF

The mathematical theory and analytical results for vibration system have been broadly reported. A series of book sections about dynamic analysis and the study of analytical DAF have been collected in [9] with related mathematical equations.

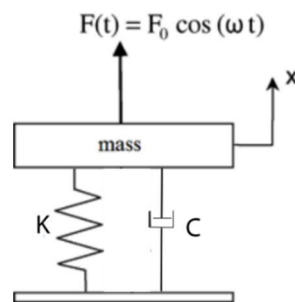


Figure 1 System forced by a harmonic external force

For instance, as stated in [10], a simplest vibration system (Figure 1) has a mass  $m$ , a spring with stiffness  $k$  and a viscous damper with the damping factor  $c$ . If such system is subject to a periodic stimulating load  $F_0 \cos(\omega t)$ , the motion of mass  $m$  shows a dynamic amplitude  $x_0$ .

The static amplitude is  $F_0/k$  since there is no consideration of mass inertia or velocity.

The ratio between dynamic amplitude  $x_0$  and the static amplitude  $F_0/k$  is calculated in Equation 4.

$$Q(\omega) = \frac{x_0}{F_0/k} = \frac{1}{\sqrt{\left(1 - \left(\frac{\omega}{\omega_0}\right)^2\right)^2 + \left(2\xi \frac{\omega}{\omega_0}\right)^2}}$$

Equation 4

where  $\omega_0 = \sqrt{\frac{k}{m}}$  ,  $\xi = \frac{c}{2\sqrt{km}}$

In case no damping, this ratio is calculated in Equation 5 as the analytical dynamic amplification factor (DAF) .

Equation 5

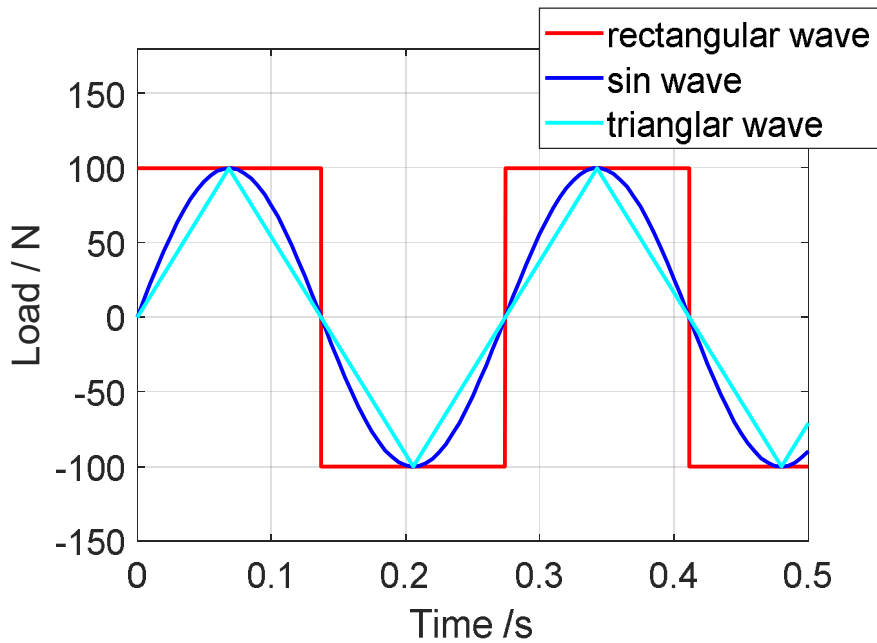
$$Q = \frac{1}{\sqrt{\left(1 - \left(\frac{f}{f_0}\right)^2\right)^2}}$$

where  $f = \frac{\omega}{2\pi}$ .

To verify the theory, a simplified forced vibration model has been built in ABAQUS (Figure 2 a) to get the numerical solution of DAF. A bar has cross section 10×10mm<sup>2</sup> and a length of 1000 mm. Young’s modulus is 210 GPa and density is zero. No damping is defined. The left end of the bar is fixed on the wall, and a mass point of 1kg is fixed on the right end.



a)



b)

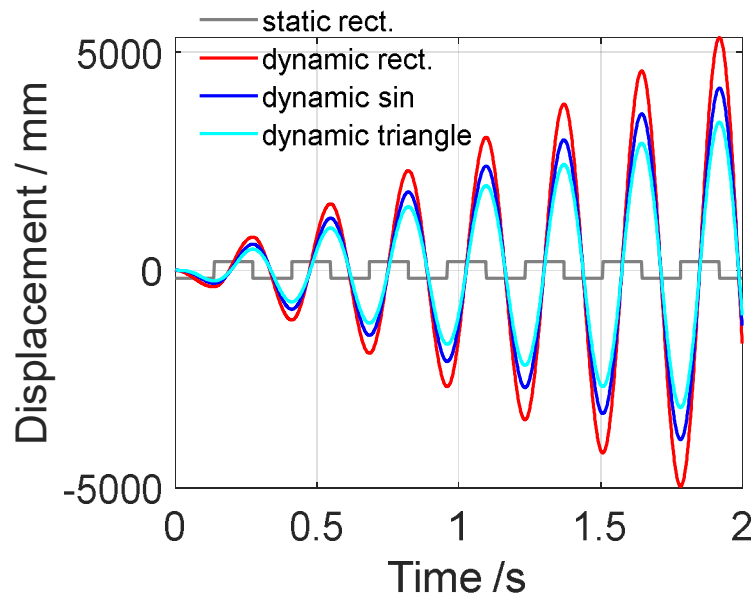
Figure 2 Massless bar and mass point a) simplified sketch, b)external load.

The mass point stays still at the beginning, and is then driven by an external periodic loading as shown in Figure 2 b). The wave form of the external loading is either rectangular, sin or triangular.

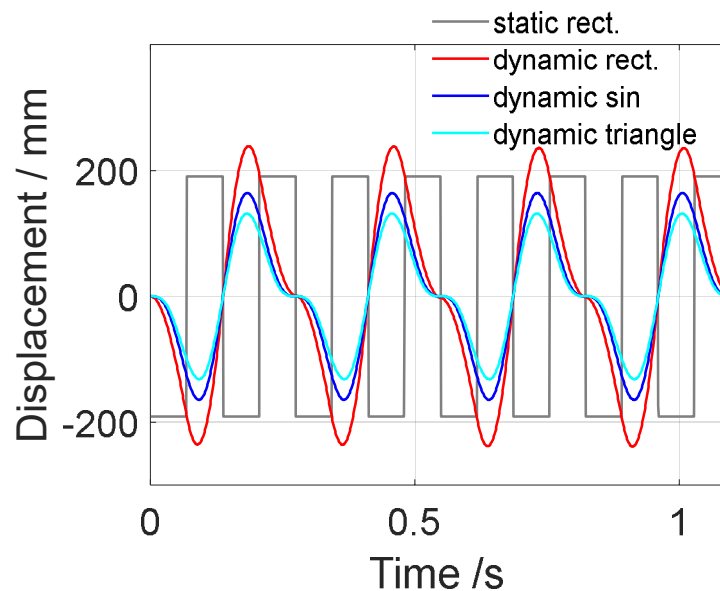
In this bar-mass point system, the stiffness of the bar is  $524.96 \text{ kg/s}^2$ , and the eigen-frequency is  $3.64656 \text{ Hz}$ .

The dynamic response with external frequency equal to eigen-frequency is shown in Figure 3 a). Since no damping has been defined, the displacement is amplified unlimitedly cycle by cycle.

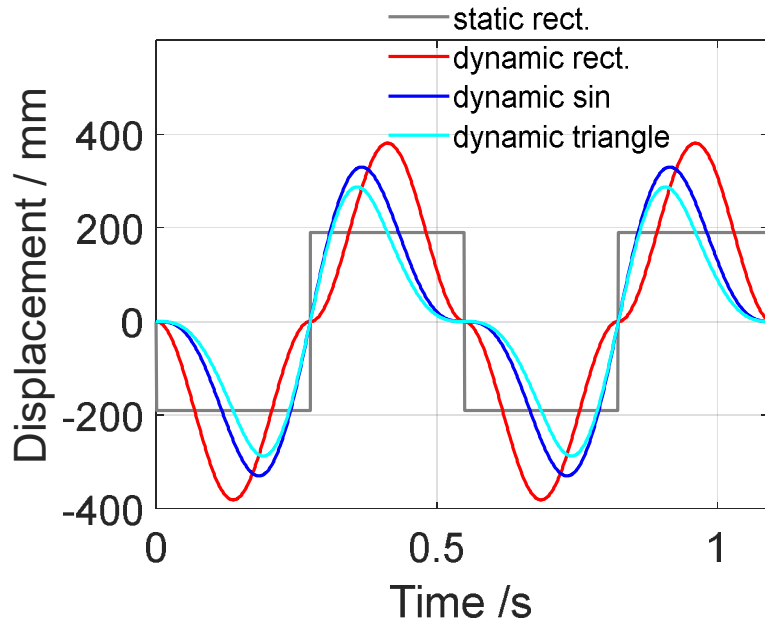
If the external loading have the twice or half of the eigen-frequency, the displacements of the mass point have been collected and shown in Figure 3 b&c). The ratio between dynamic and static amplitudes have been collected in Table 1, as well as the analytical DAF calculated through Equation 5.



a)  $1 \times$ eigen-frequency, no damping



b)  $2 \times$ eigen-frequency, no damping



c)  $0.5 \times$  eigen-frequency, no damping

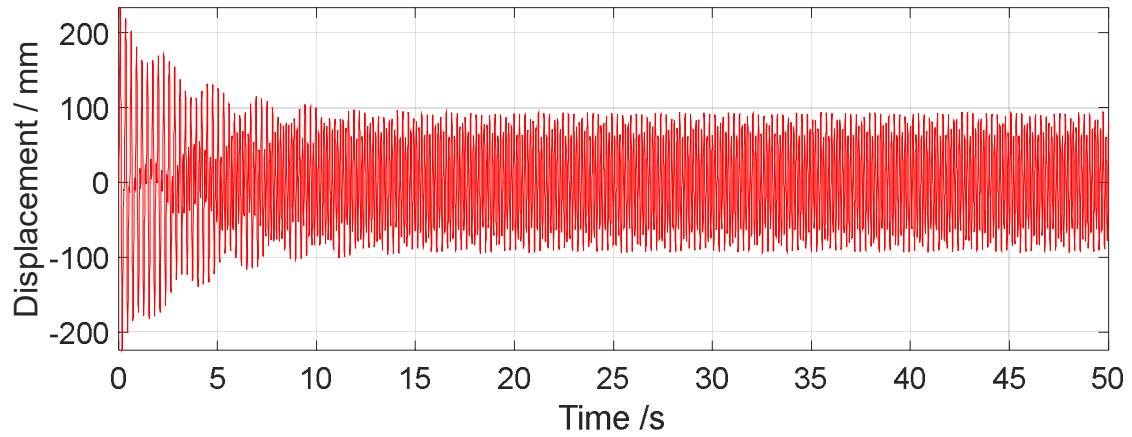
Figure 3 Displacement response of mass point, stimulation frequency

|                  | $f_{extern} = 2 \times f_{eigen}$ | $f_{extern} = 1/2 \times f_{eigen}$ | $f_{extern} = 1 \times f_{eigen}$                        |
|------------------|-----------------------------------|-------------------------------------|--|
| Analytical DAF   | 0.33                              | 1.33                                | Amplified unlimitedly cycle by cycle due to zero damping |
| Rectangular wave | 1.25                              | 2.00                                |  |
| Sin wave         | 0.86                              | 1.73                                |  |
| Triangular wave  | 0.69                              | 1.51                                |  |

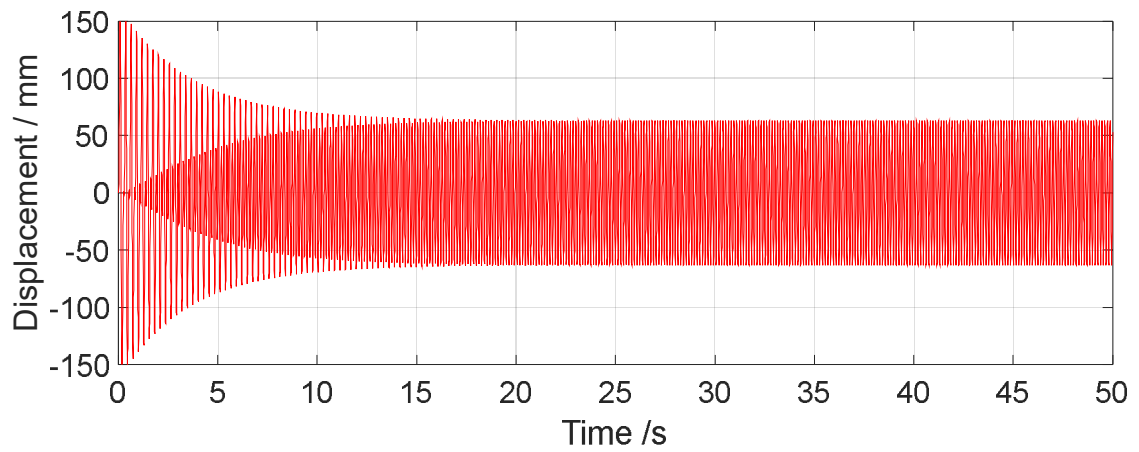
Table 1 Ratio between dynamic and static amplitudes, together with analytical DAF.

The fact is, the analytical DAF, as calculated by Equation 4 & Equation 5, is only valid for steady state response. And the external loading should have sin/cos wave form. The displacement responses shown in Figure 3 belong to initial response. Damping factor have to be introduced to transform the initial response to a steady state response.

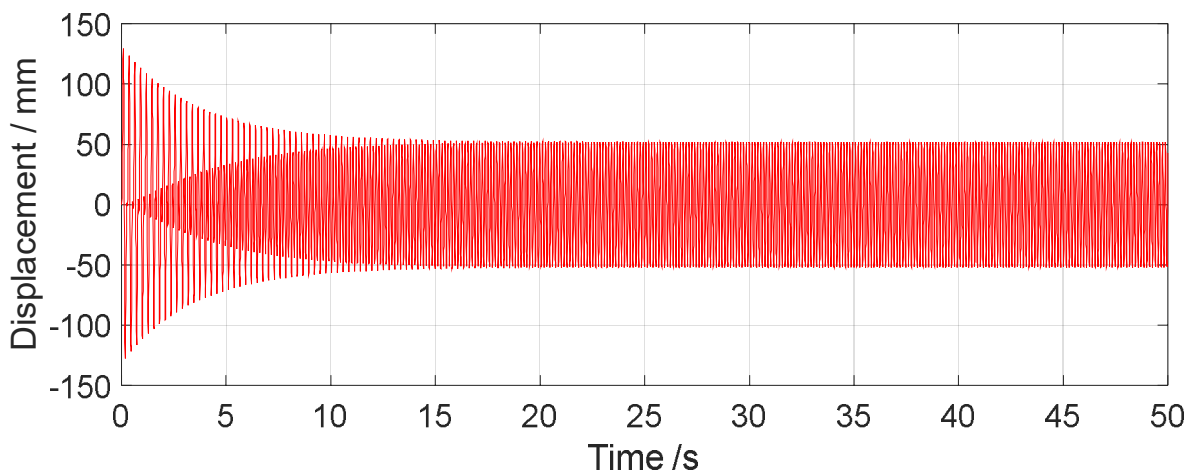
In order to reach a steady state response, while minimizing the effect of damping, another group of dynamic analysis have been performed with very small damping ratio  $\xi = 0.001$ . The frequency of the external loading is the twice of eigen-frequency, which is the same as that shown in Figure 3 b).



a) Rectangular wave



b) Sin wave.



c) Triangular wave

Figure 4 Displacement response of mass point, stimulation frequency =  $2 \times$  eigen-frequency, very low damping.

As shown in Figure 4, the displacements in dynamic analysis until 50 seconds have been collected. For all three wave forms, after around 15 seconds, the wave forms of the stimulated motions are kept the same until 50 s. The motions driven by the external sin and triangular waves show also perfect sin waves as response. The displacement response to the rectangular wave is not in sin form.

The DAFs of these three responses are as follows:

Rectangular wave : 0.480 (average)

Sin wave : 0.3318

Triangular wave : 0.2731

The DAF = 0.3318 shown in Figure 4 b) for the response to external sin wave is the closest one to this analytical value  $1/3$ .

According to the displacement responses of the bar-mass point model, the gaps between mathematical theory for analytical DAF and the numerical DAF calculated by FEM tool are concluded as follows:

1. Analytical value of DAF is only valid for steady state response.
2. Analytical value of DAF is only valid for external sin/cos wave form.

In this work, the EM loading has rare possibility to show a perfect sin/cos wave form, and the response of divertor in the initial phase, instead of steady state, is to be focused on. Therefore, the traditional analytical theory of vibration is hardly applicable for the motion of divertor under EM loading.

### 3. 3D model of DEMO divertor with FEM tool

Totally 702 CAD-parts [5] have been imported to FEM tool ABAQUS.

The dynamic analysis as well as static analysis have been set to be transient in ABAQUS. Total period of simulation is 0.5 s, while the EM loading only last for the initial 0.12 s. Data is stored by every 0.001 s. Such fine time step is to catch the peak values, as well as to get smooth curves of sub-waves of vibration.

The approximate global size of mesh is 80 mm. 10-node quadratic tetrahedron elements (C3D10) have been applied.

#### 3.1 Simplification

However, too many detailed and fine structures exist in the originally imported model [5], especially in the sub-components such as inner vertical target (IVT), outer vertical target (OVT), liner and reflector plate (RP). It would take too long calculation time to include all these fine structures in FEM analysis for DAF, and is currently not necessary.



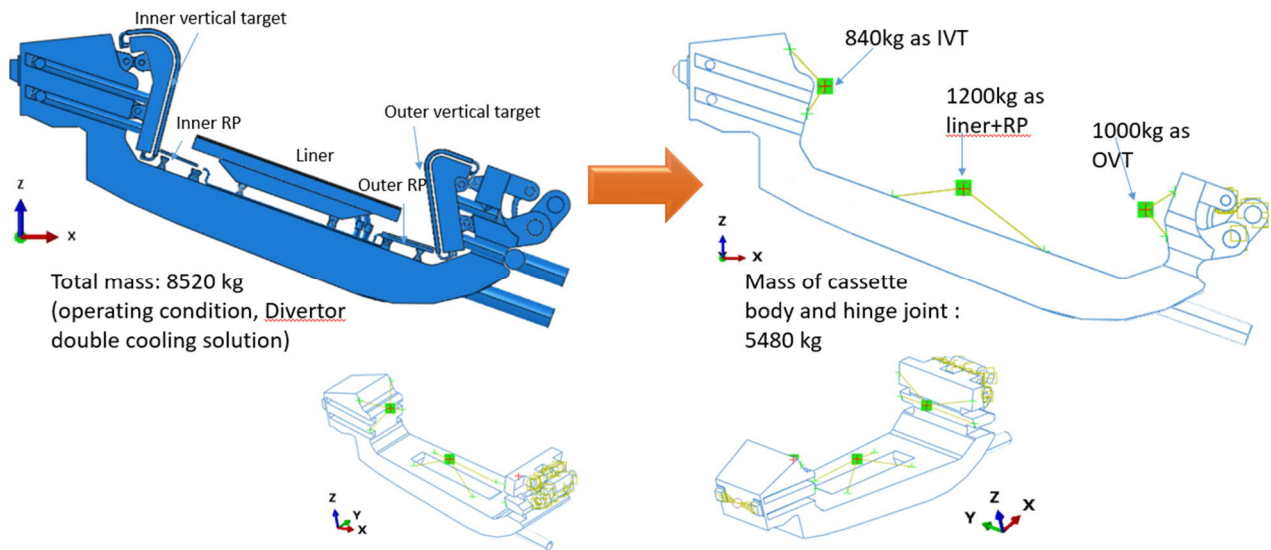


Figure 5 Simplification by replacing sub-components to mass points

To simplify the 3D model, 3 mass points have been added to replace respectively 1. IVT 2. Liner + RP 3. OVT. The positions of the mass points are located on the centers of mass of the corresponding sub-components. The coordinates and weights of these mass points have been illustrated in Figure 5.

The weights of the mass points are approximately estimated according to EUROfusion internal data base for double cooling solution with the mass of water. And on the other hand, the weights of mass points are to fill the gap between 8.52 Ton as the total mass of divertor in operating condition and 5.48 Ton as the mass of left components: cassette, wishbone and three pins of the hinge joint.

Equation 6 
$$8.52 \text{ Ton} - 5.48 \text{ Ton} = 0.84 \text{ Ton} + 1.2 \text{ Ton} + 1 \text{ Ton}$$

with

- 8.52 Ton : reported total mass of divertor in operating condition
- 5.48 Ton: calculated mass of cassette body and hinge joint by FEM software
- 0.84 Ton, 1.2 Ton and 1 Ton : estimated masses of IVT, liner + RP, OVT with mass of water

The mass of water is included into the 3 mass points.

Note that in the future work, the representative moment of inertia of these sub-components shall be added.

Further, in the original CAD model, there have been many holes for inlet / outlet on the cassette body. Too many fine meshed elements have been found around these holes, which leads to unnecessarily too large number of elements, since these holes are believed to have marginal effect on the analysis for vibration of the whole structure.

Hence further simplification has been performed by filling out these holes. The number of meshed elements have been significantly reduced, from over 90 thousand to around 30 thousand.

### 3.2 Fixation

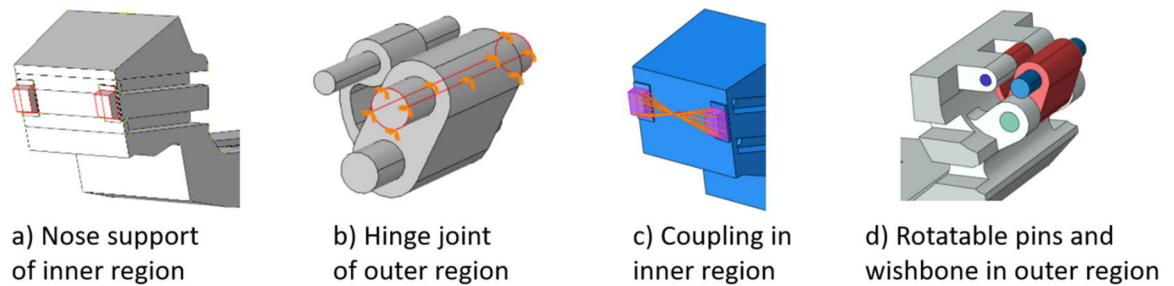


Figure 6 Fixation of the cassette body

The cassette body is supported by a nose support in the inner region (Figure 6 a) and by hinge joint in the outer region (Figure 6 b) to provide elastic compliance for preloading and for compensating the mismatch of differential thermal strains between cassette body and vacuum vessel [2].

The surfaces of the nose support (pink in Figure 6 c) are coupled to a reference point. Then this reference point is fixed in X / Y / Z - displacement and X / Y / Z - rotation.

The pin of the hinge joint (Figure 6 b), which is connected to the vacuum vessel (VV), applies an initial displacement for preload and then is fixed to ground. Rotation and translation between this pin and wishbone is allowed with friction.

The other two pins connecting to the cassette can rotate and translate within the holes with friction.

In the result section of this report, four groups of results with different fixation-setup for the hinge joint in ABAQUS are presented, under the concept of Parametric Digital Model Development[8]. More detailed information of fixation has been collected in Table 2.

### 3.3 Material

Three material properties are necessary in the dynamic analysis: density, Young's modulus and Poisson's ratio. The current EUROfusion MPH of Eurofer97 [11, 12] has been applied to the model.

The CAD is supposed to be built based on the dimension at room temperature, hence  $7.744 \text{ g/cm}^3$  as the density of Eurofer97 at  $20^\circ\text{C}$  has been applied.

The Young's modulus between  $200^\circ\text{C}$  and  $250^\circ\text{C}$ , as the operating temperature range [2], has been applied to the model, which is 205 GPa.

Poisson's ratio is set to be 0.3 as suggested in MPH of Eurofer97.

Note that, in the future work, the material for wishbone shall be replaced by Ti-6Al-4V. And the material for the pin shall be replaced by Inconel 718 [13].

In the analysis group III and IV, friction coefficient is set to be 0.31, according to kinetic coefficient between Ti-6Al-4V and 17-4 stainless in the environment air or vacuum [14].

Damping ratio 5 % is included in the analysis group III and IV. Although it is 4 % according to [4], this value shows rare influence to the result of current work, since only the initial period of stimulated vibration of divertor is considered.

### 3.4 Preload

A preload of 60 kN pointing from the fixed pin joint (Figure 6 b) to the nose support (Figure 6 a) is to be applied by an initial displacement of this fixed pin joint (Figure 6 b). Such preloading through so-called outer-locking mechanism is to remove any clearances and avoid “shaking” due to sudden change of the magnetic field [15].

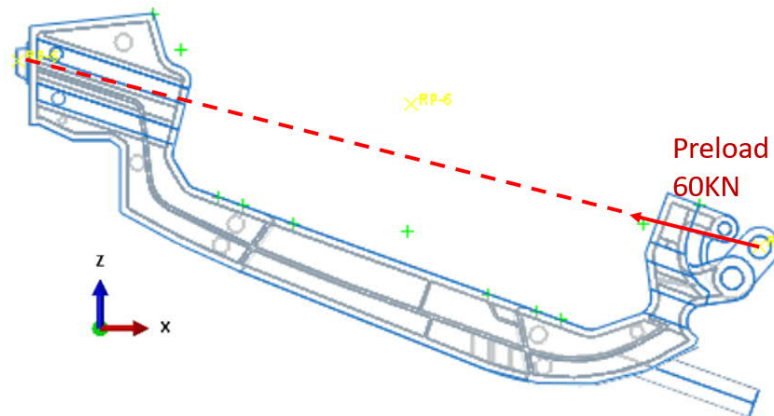


Figure 7 Preload 60 kN is applied by an initial displacement, starting from the pin connecting to VV, to the nose support.

As shown in Figure 7, an initial displacement is applied to generate a preload of 60 kN. The relation between this displacement and the reaction force on the nose support is linear.

However, such preload is raised to be over 200 kN in group III and IV, to make sure that the reaction force of the nose support in X-direction is always over zero, meaning the nose support is always under compression. This is achieved by raising the displacement ( $\Delta x = -0.4823$  mm,  $\Delta z = 0.1206$  mm) to higher displacement ( $\Delta x = -1.60767$  mm,  $\Delta z = 0.402$  mm). Note that, due to different setups of boundary conditions in the four groups, the displacement induced preloads are not always the same.

### 3.5 EM loading

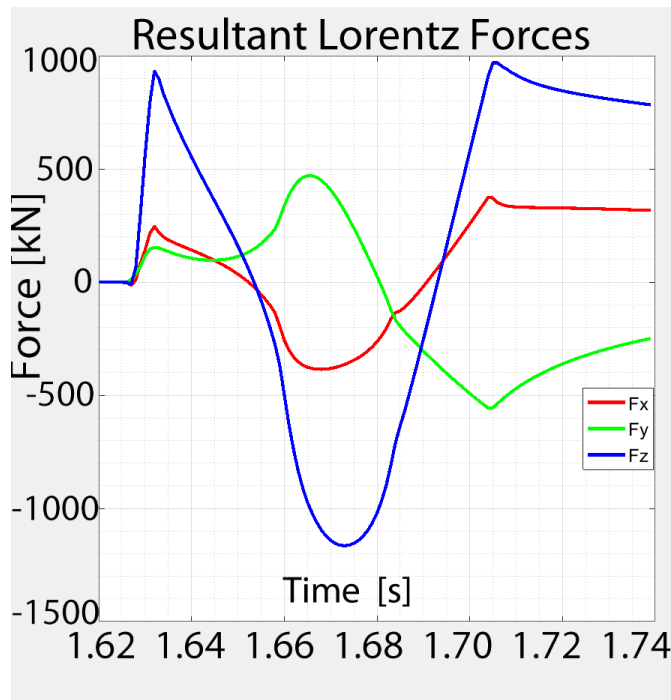


Figure 8 Resultants of the Lorentz forces referred to the whole divertor [1]

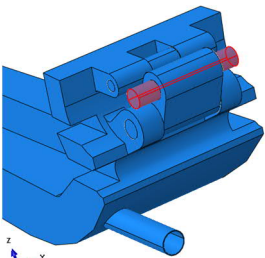
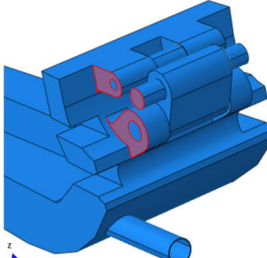
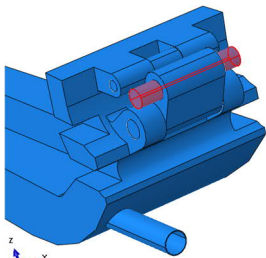
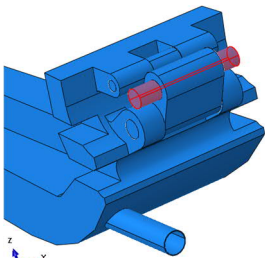
Lorentz forces (Figure 8) in three directions X, Y, Z have been applied to the 3D model as an example of external loading, to compare the displacement responses in static & dynamic FEM analysis. Time step in analysis is 0.001 second as mentioned above.

Note that, in the current analysis, Lorentz forces are evenly distributed on the whole body as volume force. However, in the real case, this distribution is not even and will generate moments.

For the current work, moments are not accounted. In future work, the analysis of motion of divertor under EM loading is to be updated with new results of Lorentz forces as well as moments.

### 3.6 Summary of boundary conditions in four group of analysis

**Table 2** has collected the most significant information about the boundary conditions in the four groups of analysis, in order to make highlight on the differences of settings in FEM software ABAQUS between these four groups.

| Group I  | Group II   | Group III   | Group IV   |
|--|--|---|--|
|  <p>Pin to VV all-fixed</p> |  <p>Surfaces of joints fix in Y</p> |  <p>Pin to VV all-fixed</p> |  <p>Pin to VV all-fixed</p> |

|   |   |  |   |
|---|---|--|---|
| Friction 0.1<br>Zero damping<br>60 kN by displacement | Friction 0.1<br>Zero damping<br>60 kN by displacement | Friction 0.31<br>Damping 0.05<br>217 kN by displacement<br>-300 kN in X-axis EM<br>preload | Friction 0.31<br>Damping 0.05<br>251 kN by displacement<br>-300 kN in X-axis EM<br>preload<br>3 * Young's modulus<br>wishbone |
|---|---|--|---|

Table 2 Summary of boundary condition in the four groups of FEM analysis

## 4. Results

### 4.1 Frequency analysis

| Mode | Eigen-Frequency (Hz) Group I | Eigen-Frequency (Hz) Group II | Eigen-Frequency (Hz) Group III | Eigen-Frequency (Hz) Group IV |
|------|------------------------------|-------------------------------|--------------------------------|-------------------------------|
| 1    | 61.700                       | 93.542                        | 63.080                         | 69.085                        |
| 2    | 92.949                       | 107.11                        | 93.076                         | 96.189                        |
| 3    | 147.53                       | 150.64                        | 149.31                         | 156.77                        |
| 4    | 152.44                       | 190.23                        | 152.73                         | 157.93                        |
| 5    | 188.75                       | 190.85                        | 188.91                         | 201.95                        |
| 6    | 203.65                       | 241.45                        | 203.03                         | 214.97                        |
| 7    | 238.56                       | 246.18                        | 240.61                         | 249.50                        |
| 8    | 244.14                       | 256.85                        | 244.48                         | 249.87                        |
| 9    | 252.44                       | 324.70                        | 252.96                         | 272.53                        |
| 10   | 333.37                       | 362.53                        | 333.49                         | 334.39                        |

Table 3 Summary of calculated eigen-frequencies in the four groups of analysis.

The eigen-frequencies of the initial 10 modes in the four groups of analysis have been collected in Table 3. The frequency of external EM loading lies around 15 Hz (Figure 8) which is already lower than the eigen-frequencies in the 1<sup>st</sup> mode. Hence no resonance can be generated, and it is not necessary to consider further modes with even higher eigen-frequencies.

The eigen-frequencies of group I, III and IV are similar, especially those of group I and III have only marginal differences. This indicates that friction, damping and preload have rare effect on eigen-frequency.

The calculated eigen-frequencies of group II is however very different from the other three groups, because the surfaces of joints in outer region have been fixed in Y-direction, as shown in Table 2.

The displacements of the first two modes are shown in Table 4, with automatic amplification of the deformation for better illustration.

|                         | Mode 1 | Mode 2 |
|-------------------------|--------|--------|
| Group 1<br>U, Magn.<br> |        |        |
| Group 2                 |        |        |
| Group 3                 |        |        |
| Group 4                 |        |        |

Table 4 Illustration of displacements of the first two modes in each group of analysis

As similar to the calculated eigen-frequencies in Table 3, the distribution of the displacements of group I, III and IV are also comparable, while the displacements in group II are quite different from the others due to the fixation of the surfaces of joints in the outer region in Y-direction (Table 2).

## 4.2 Dynamic and static analysis of 3D model with external loading

As shown in Table 4, the bottom of cassette body generally has higher displacement. Hence the displacement responses of one node (Node Nr. 8279) on the bottom and on the y-symmetric plane in dynamic & static FEM analysis have been collected and compared as an example since this node is lowest one in Z - direction. Note that, this node does not necessarily have the maximum vibration among all nodes of the mesh.

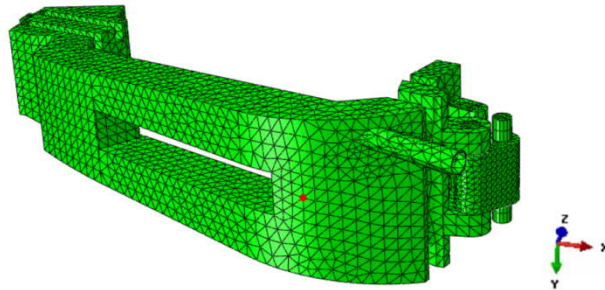
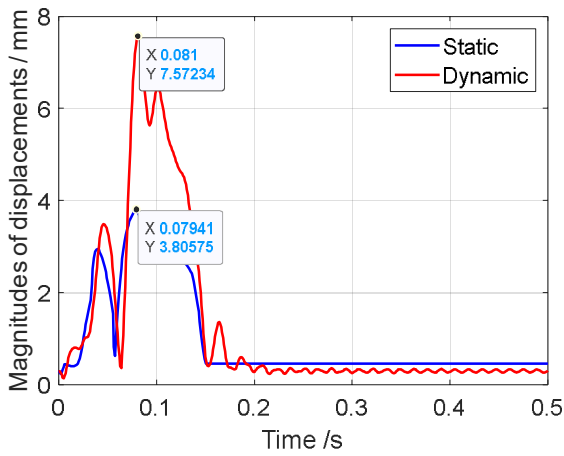


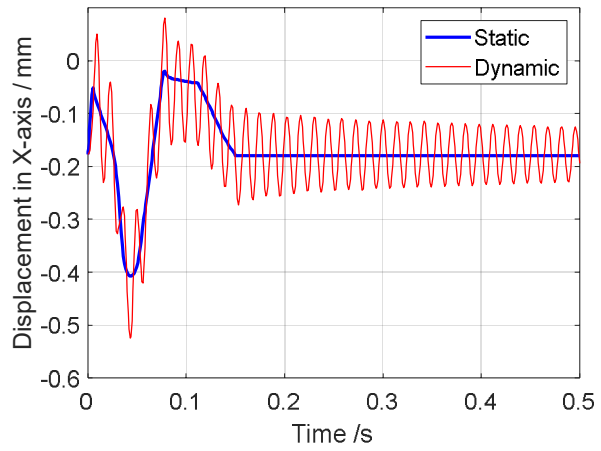
Figure 9 Node Nr.8279 on the bottom of cassette body

### 4.2.1 Group I result

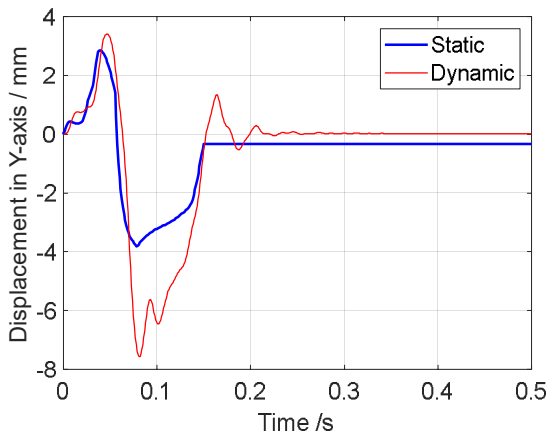
The displacements of node Nr. 8279 in the first group have been recorded and shown in Figure 10.



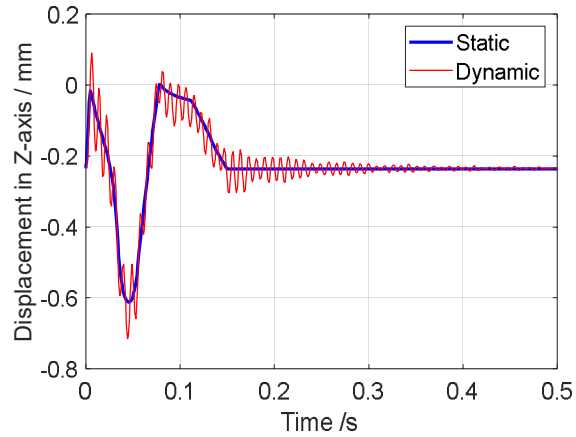
a) Displacement magnitude



b) Displacement in X-axis



c) Displacement in Y-axis



d) Displacement in Z-axis

Figure 10 Displacements in X,Y,Z-directions and magnitudes of node Nr.8279 under combined Lorentz forces, in dynamic and static analysis, group I.

In direction X and Z, sub-waves have been found in the dynamic displacements (red curves). The static displacements (blue curves) go along the dynamic sub-waves as mid-lines. In Y-axis, it is hard to determine a steady sub-wave.

The frequency of sub-wave in X-axis is 71 Hz. And the frequency of sub-wave in Z - axis is 123.4 Hz. This is however different from the eigen-frequencies calculated in frequency analysis, as collected in Table 3.

The magnitude of displacement in Y-axis is apparently higher than those in X- and Z-axis, since the wishbone is able to slide on the pin connecting to VV with very low friction coefficient 0.1.

The peak magnitude of combined displacement in dynamic analysis is 7.57 mm, while the one in static analysis is 3.8 mm. The ratio in between is  $1.987 \approx 2.0$ .

Referring to the objective of this work, a DAF is to amplify the loading in the static analysis, and to make the static displacement be over the dynamic one (Equation 3).

Therefore, the Lorentz forces (Figure 8) in all three directions have been amplified by factor 2.0 in a further static FEM analysis. The displacement magnitude of node Nr. 8279 in this further static analysis has been recorded and compared with the one in the previous dynamic analysis, as shown in Figure 11.



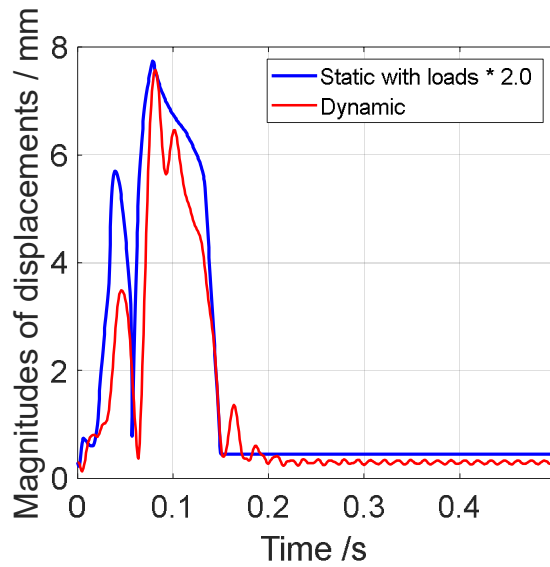


Figure 11 Dynamic displacement compared with static displacement of node Nr.8279 with amplified loading, group I.

With the amplified external loading, the calculated displacements (blue curve in Figure 11) in static FEM analysis is now mostly over the dynamic ones with original external loading (red curve in Figure 11). This meets the objective of this work.

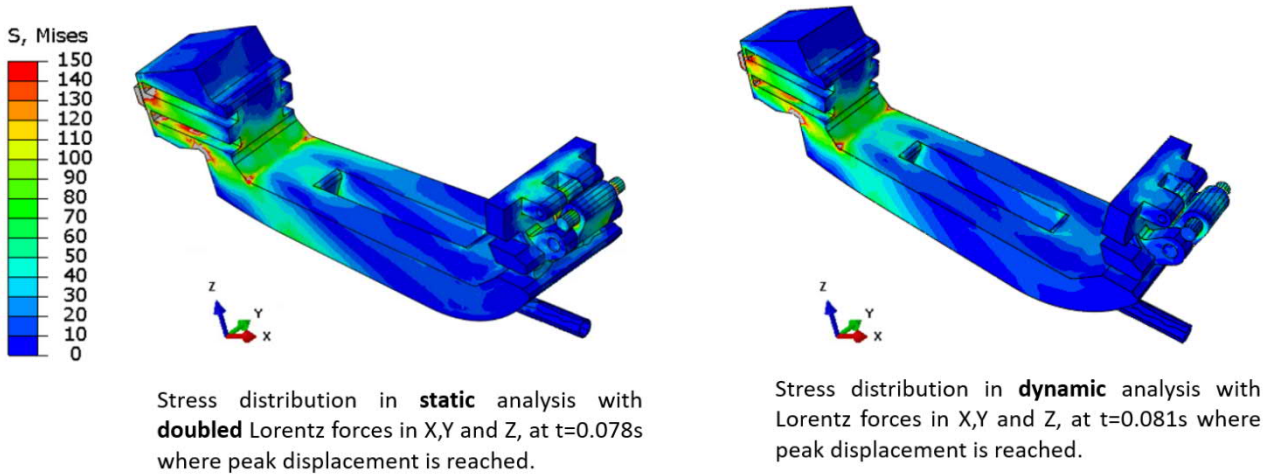


Figure 12 Comparison between the stress distribution in static analysis with amplified loading and in dynamic analysis

The stress profiles of the static analysis with doubled Lorentz forces, and the one of dynamic analysis have been compared, as shown in Figure 12. These two stress profiles are generally similar. Hence, not only the strains/displacement in amplified static analysis, but also the stresses have been amplified to be over those in dynamic analysis.

However, such doubled Lorentz force cannot guarantee that Equation 2 for stress is valid for every location on the divertor.

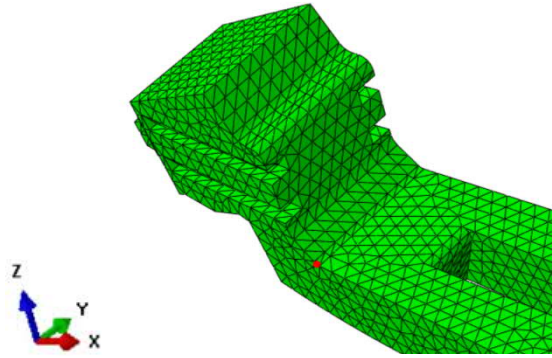


Figure 13 Node Nr. 50330 (red point)

It is found in Figure 12 that, there is stress concentration at the edge, which is close to node Nr. 50330 (Figure 13). The stresses of this node in the static analysis with amplified loading and in dynamic analysis have been compared, as shown in Figure 14.

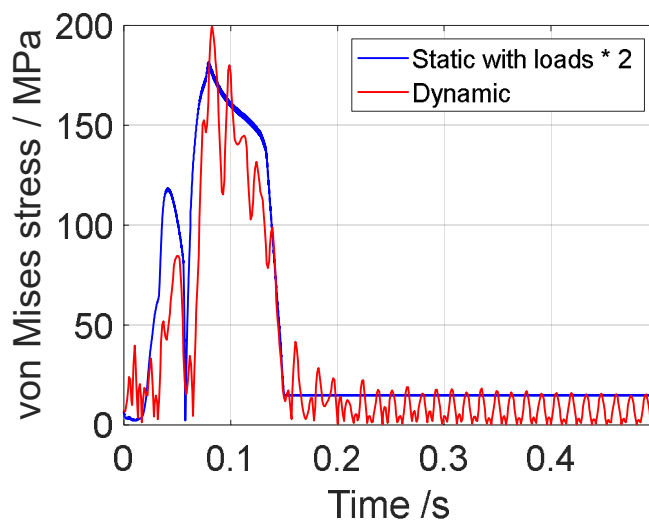


Figure 14 von Mises stress of node Nr. 50330 in amplified static analysis and in dynamic analysis.

With the amplified loading, the von Mises stresses in static analysis are mostly over the stresses in the dynamic analysis. However, such doubled loading cannot guarantee that Equation 2 is valid for every time point.

The boundary conditions (Table 2) in the current group make the wishbone slide quite freely along the pin connecting to VV due to minimized friction, and consequently make the motion of cassette body in Y-direction contributes the larger part to the total magnitude of displacement.

In the following three groups of simulations, the motion in Y-direction will be restricted to evaluate the resulted change of DAF. It will be done either by fixing the Y-motion of the joint of cassette to wishbone directly (Group II), or by increasing the friction coefficient (Group III, IV)

#### 4.2.2 Group II result

In this group of tests, several section of surfaces of joints in outer region have been fixed in Y-direction (Table 2). Although these restrictions are not part of the current design, it is worthwhile to find a limit for DAF with mostly restricted motion.

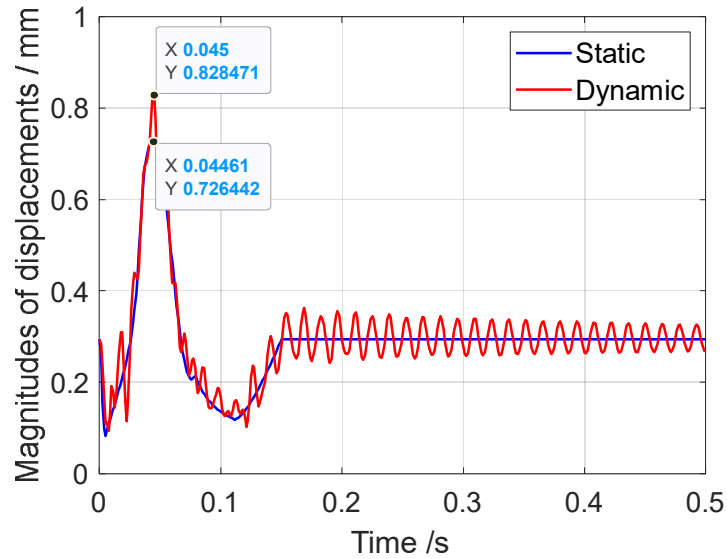


Figure 15 Magnitude of displacements of node Nr.8279 under combined Lorentz forces, in dynamic and static analysis, group II.

The peak magnitude of displacement in dynamic analysis is 0.8285 mm, while the one in static analysis is 0.7266 mm. After the initial displacement 0.2944 mm is subtracted, the ratio in between is:

Equation 7 
$$(0.8285 - 0.2944) / (0.7266 - 0.2944) = 1.23$$

A further static analysis has been performed with amplified EM loading by this ratio = 1.23.

However, as shown in Figure 16, the peak magnitude of static displacement with amplified loading by 1.23 (black curve) is still lower than that in dynamic analysis, although very close. Unlike the doubled loading in group I, if the external loading is amplified only by this ratio (1.23) between dynamic and static displacement in the current group II, it is not enough to meet the objective stated in Equation 3. Therefore, the loading is further amplified by 1.3 and 1.4.

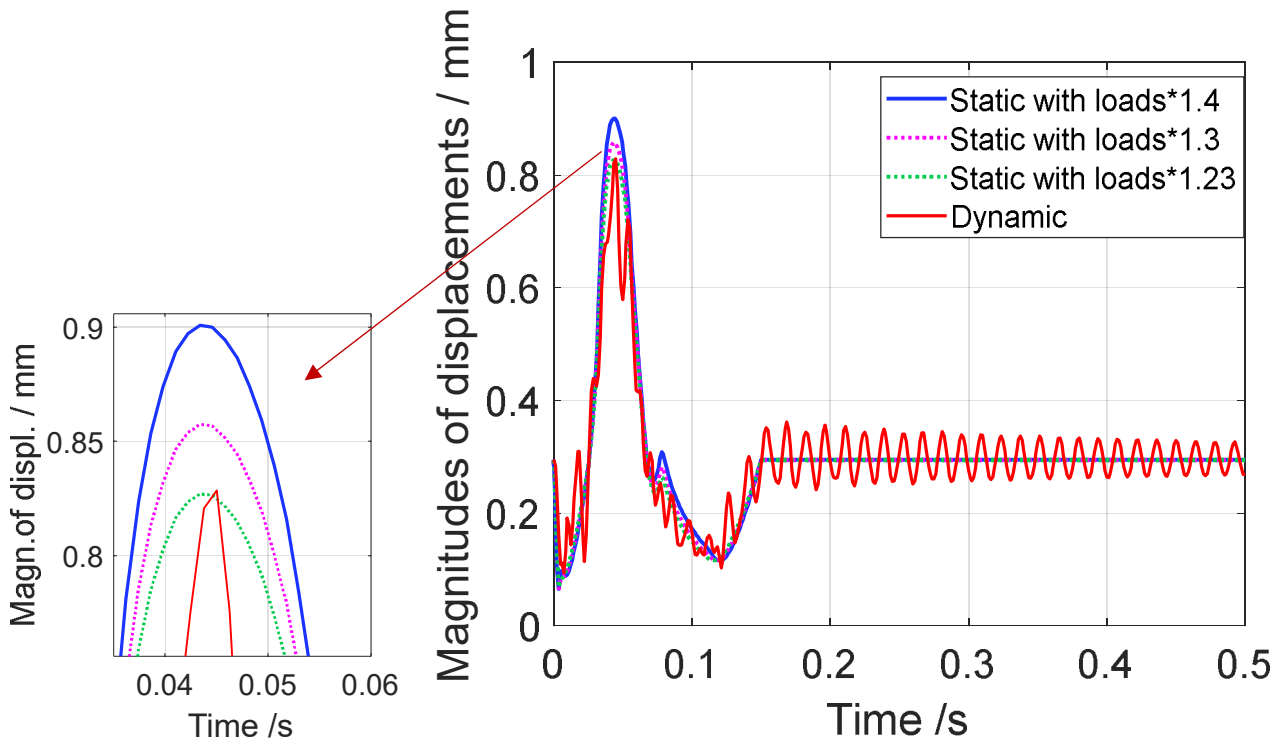


Figure 16 Dynamic displacement compared with static displacement of node Nr. 8279 with amplified loading, group II.

It shows that, with amplification factor 1.3 and 1.4, the peak static displacement can be clearly over the dynamic one.

Nevertheless, in spite of the peak displacement, all these amplified static displacements are mostly over the dynamic ones.

The stress profiles have been further checked.

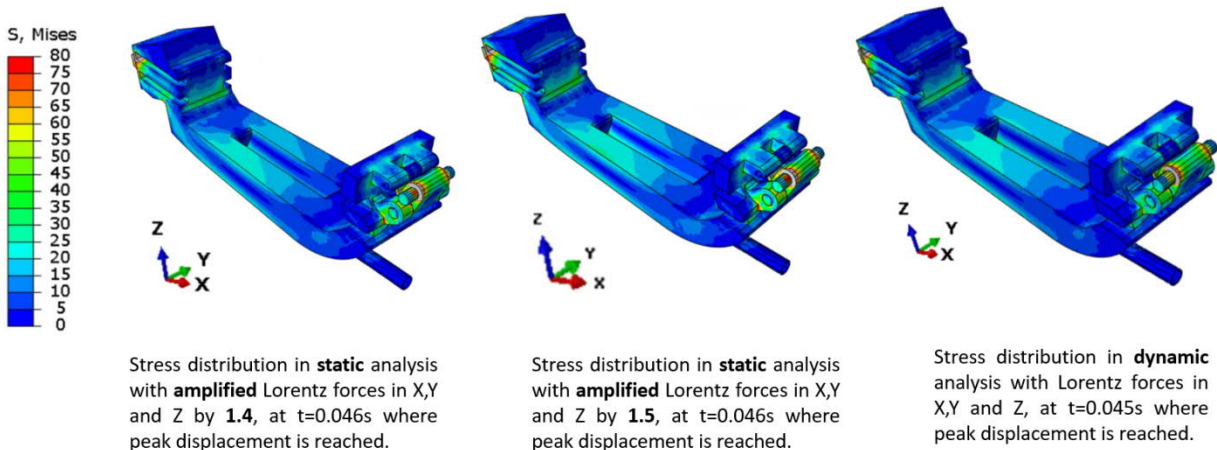


Figure 17 Stress profile of amplified static analysis and dynamic analysis, group II.

The distributions of von Mises stress in amplified static analysis with factor 1.4 and 1.5, as well as the one in dynamic analysis are shown in Figure 17. Although these three stress profiles have in between only marginal differences, the one with DAF = 1.5 is closer to the dynamic stress profile.

For the time being, DAF = 1.5 is suggested for this group II. However, if the stress in the static analysis must be over the dynamic one for every location at every time point (Equation 2), factor 1.5 is still not enough.

### 4.2.3 Group III result

In this group of analysis, two preloads have been added, which are 217 kN by initial displacement and 300 kN ferromagnetic preload. Such preloads ensure that the cassette is always pushing the nose support (Figure 6 a).

The setups of fixation are similar to those in group I, but the friction coefficient has been increased from 0.1 to 0.31, as mentioned in section 3.3.

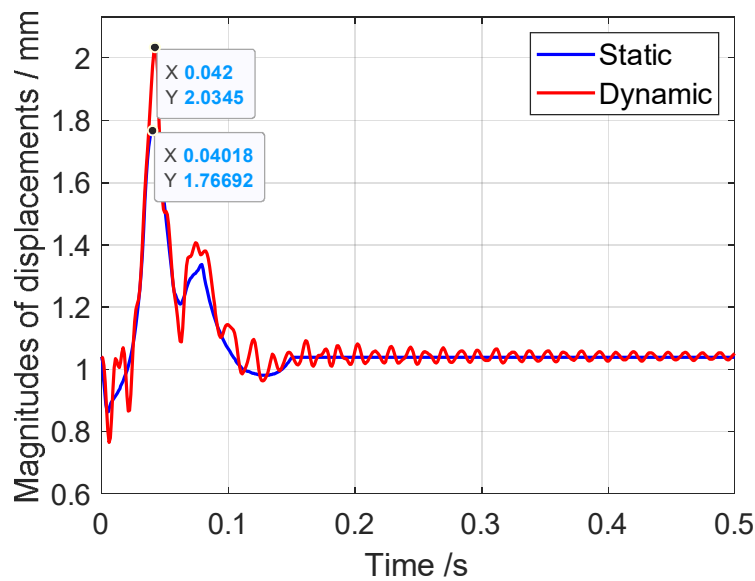


Figure 18 Magnitude of displacements of node Nr.8279 under combined Lorentz forces, in dynamic and static analysis, group III.

The ratio between the peak magnitudes of displacements in dynamic and static analysis is

$$(2.0345 - 1.03921) / (1.76692 - 1.03921) = 1.3677$$

After amplifying the external loading (Figure 8) by factor = 1.3677 in static analysis, the displacement of Node Nr. 8279 is recorded and compared with those of the dynamic analysis with original loading.

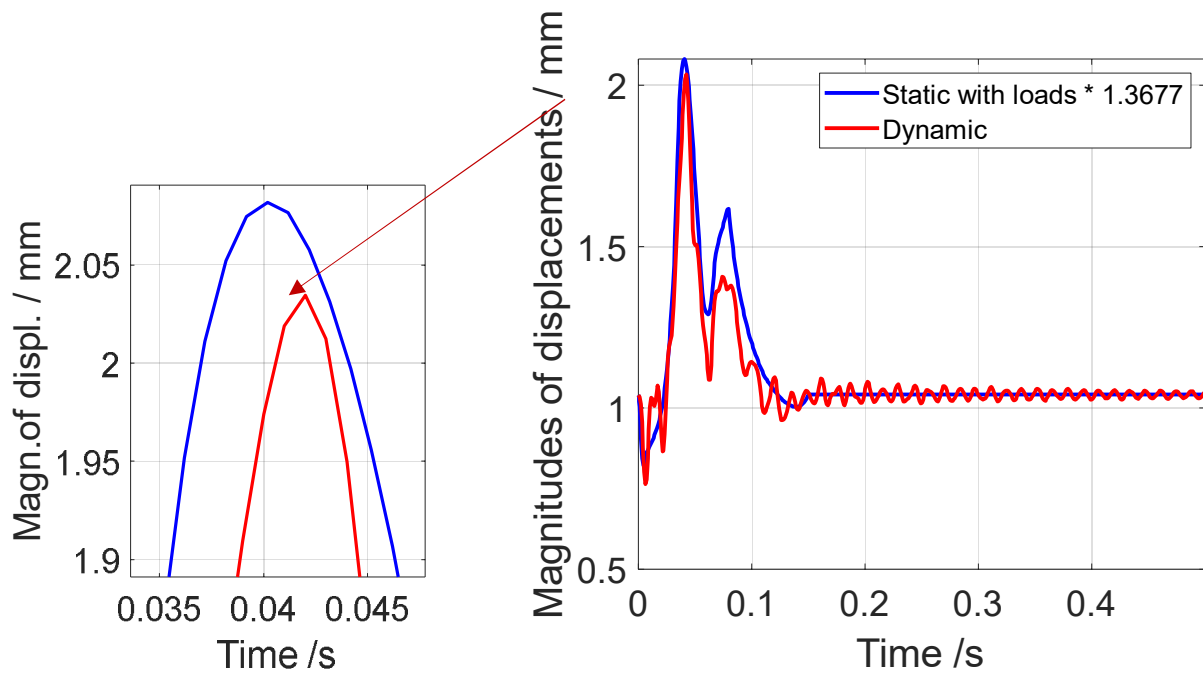


Figure 19 Dynamic displacement compared with static displacement of node Nr. 8279 with amplified loading by 1.3677, group III.

As shown in Figure 19, the amplified static displacement by factor 1.3677 is already over the dynamic displacement.

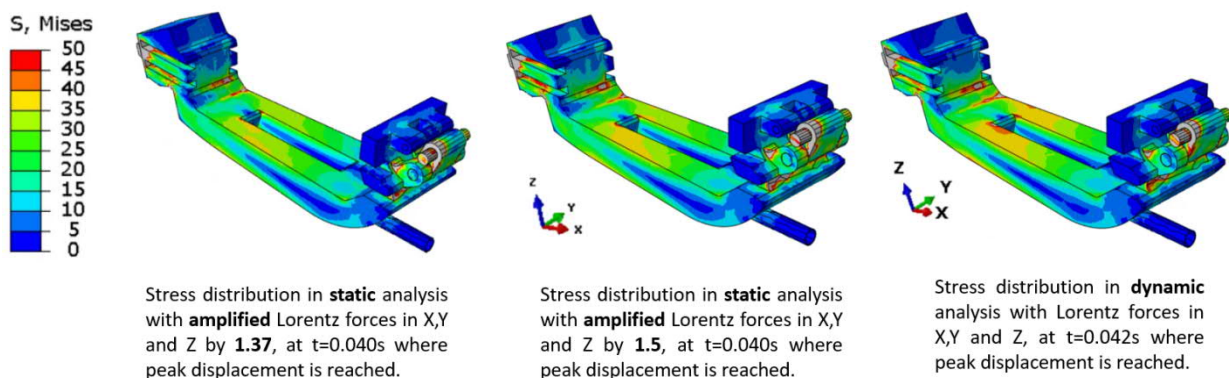


Figure 20 Stress profiles of amplified static analysis and dynamic analysis, group III.

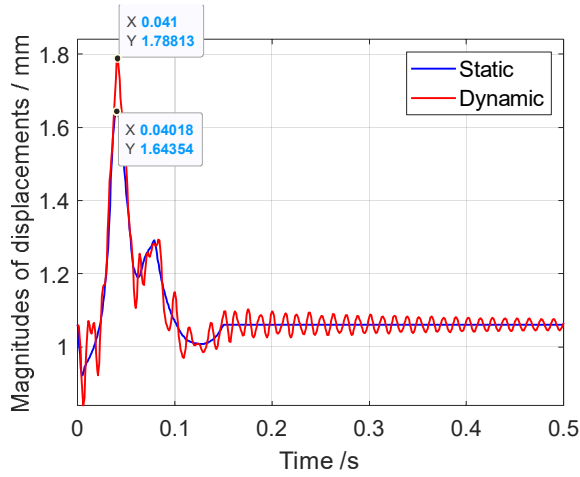
However, comparing the stress profiles in Figure 20, the amplified static stress profile with DAF = 1.37 is lower than the dynamic one for many locations. The static stress profile with DAF 1.5 is closer to the dynamic one, but still cannot not ensure that amplified static stress is over the dynamic stress for every location.

DAF = 1.5 is suggested for this group III for the time being. As the same as group II, if the stress in the static analysis must be over the dynamic one for every location on the divertor, DAF = 1.5 shall be further raised.

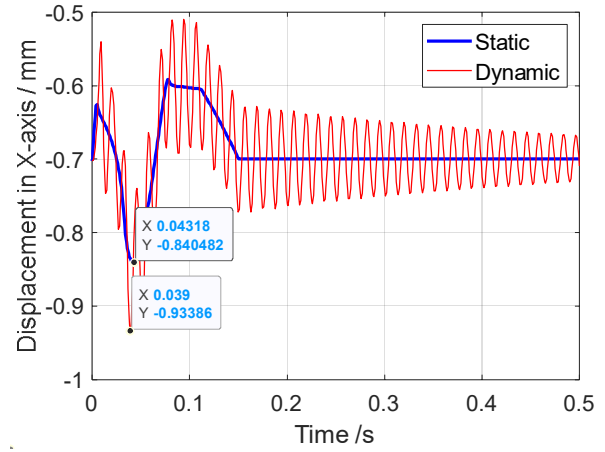
#### 4.2.3 Group IV result

The setups of boundary conditions in this group IV are currently supposed to be the closest to the actual designed divertor, as listed in Table 2.

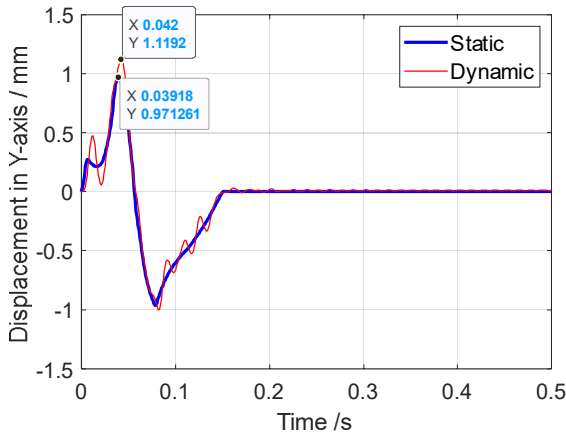
Two preloads (251 kN by initial displacement+ 300 kN ferromagnetic preload) have been applied to ensure the cassette is always pushing the nose support (Figure 6 a).



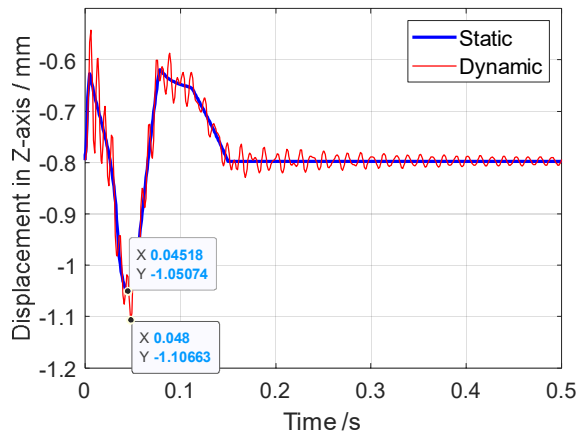
a) Magnitude



b) X-direction



c) Y-direction



d) Z-direction

The ratios of separate directions are as follows:

$$X: \quad (0.93386 - 0.70233) / (0.84048 - 0.70233) = 1.6759$$

$$Y: \quad 1.1192 / 0.9712 \quad = 1.1523$$

$$Z: \quad (1.10663 - 0.79559) / (1.05074 - 0.79559) = 1.21905$$

The ratio between the peak magnitudes of displacements in dynamic and static analysis is

$$(1.78813 - 1.06124) / (1.64354 - 1.06124) = 1.248$$

The external loading are firstly amplified by factor 1.248 for all three directions in static analysis, as the same as the previous three groups. The magnitudes of displacements of node Nr. 8279 (Figure 9) in this amplified static analysis and in the dynamic analysis are collected and shown in Figure 21.

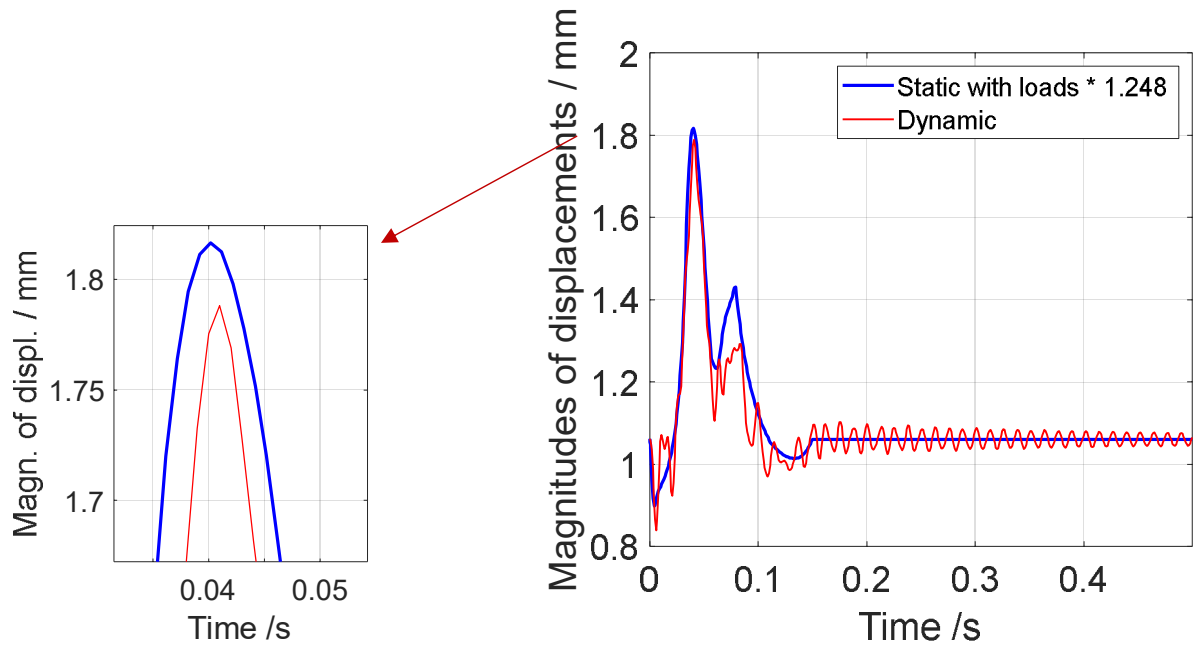


Figure 21 Dynamic displacement compared with static displacement of node Nr. 8279 with amplified loading by factor 1.248, group IV.

For this current group IV, the external loading are also amplified anisotropically, meaning the Lorentz forces in X, Y and Z (Figure 8) are respectively amplified by the following factors

$$DAF_x = 1.6759, \quad DAF_y = 1.1523, \quad DAF_z = 1.21905$$

The results are shown in Figure 22.

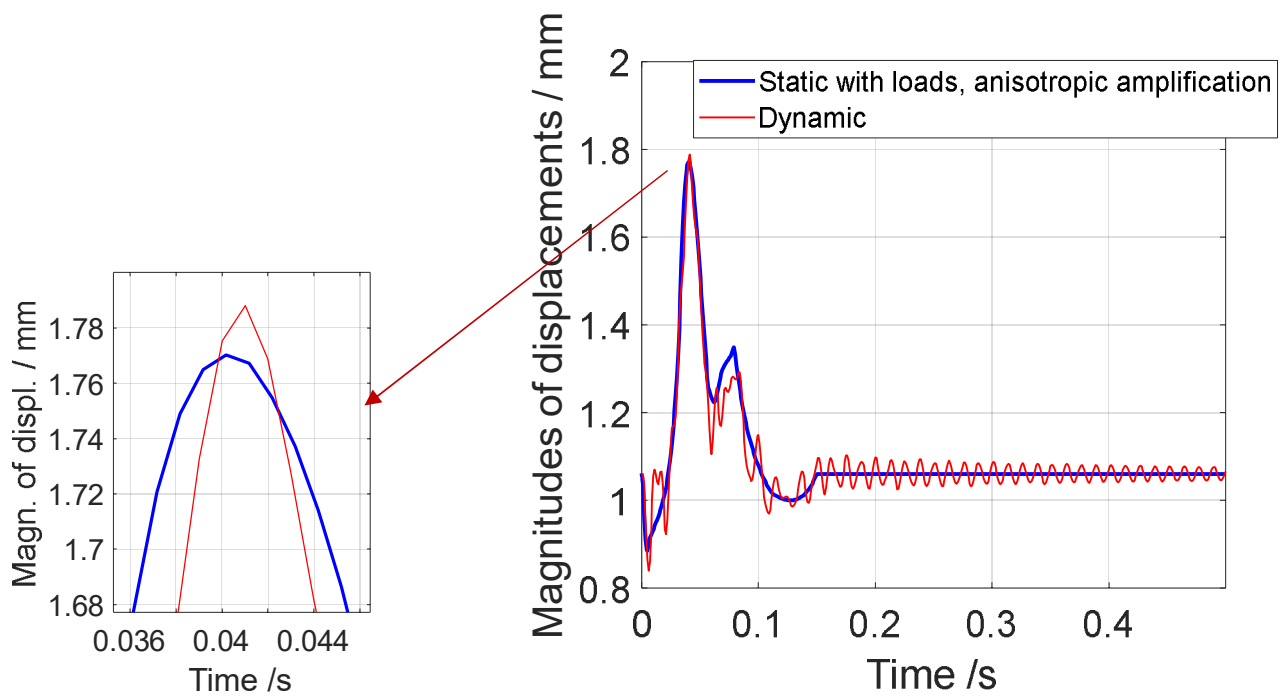




Figure 22 Dynamic displacement compared with static displacement of node Nr. 8279 with anisotropically amplified loading, group IV.

In the above two ways of amplification, both have made the static displacements be very close to the dynamic ones, for at least this node Nr. 8279 (Figure 9).

However, if the peak displacements are to be emphasized, the anisotropic amplification is not enough to make the peak static displacement to be over the dynamic one.

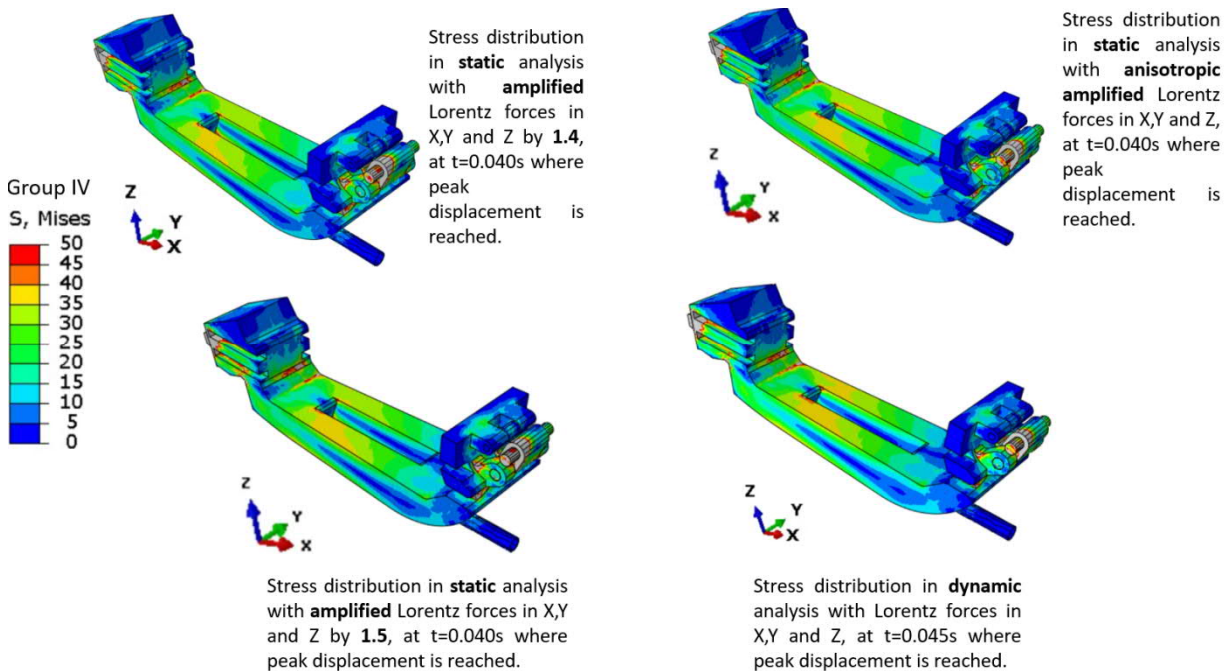


Figure 23 Stress profile of amplified static analysis and dynamic analysis, group IV.

Comparing the stress profiles shown in Figure 23, the isotropic amplification by factor 1.4 and anisotropic amplification with various factors for each direction still cannot make the static stress be over the dynamic stress for every position on cassette body. Isotropic amplification by factor 1.5 makes the stress profile closer to the dynamic stress profile.

As the same as the situation in group II and group III, for the time being, DAF = 1.5 is suggested for this group IV.

## 5. Summary and discussion

Four groups of FEM simulations have been performed with different setups of fixation to search for a conservative value of DAF under the concept of Parametric Digital Model Development [8].

One node on the bottom of cassette body has been focused on, which is numbered 8279 in the meshed 3D ABAQUS model (Figure 9). The displacement responses of this node in static as well as in dynamic FEM analysis have been recorded and compared.

|  | Group I | Group II | Group III | Group IV |
|--|---------|----------|-----------|----------|
| Peak magnitude of dynamic displacement | 7.56 mm | 0.82 mm  | 2.03 mm   | 1.79 mm  |

|  |      |      |      |      |
|--|------|------|------|------|
| Ratio of dynamic / static peak magnitude of displacement | 1.99 | 1.23 | 1.37 | 1.25 |
| Suggested DAF  | 2.0  | 1.5  | 1.5  | 1.5  |

Table 5 Summary of ratios between magnitudes of displacements in dynamic & static analysis, and suggested DAF for the four groups with various setups of boundary conditions.

As summarized in Table 5, the peak displacement of this node Nr. 8279 in group I shows the highest value (7.56 mm) since the fixation of group I is the freest one. On the opposite, the peak displacement of group II is the lowest (0.82 mm), due to the firm-fixation of several surfaces (Table 2) of the joint in Y-direction. The fixations of group III and IV approach the actual designed fixation, no firm-fixation like in group II, with friction coefficient 0.31 which is higher than coefficient 0.1 in group I. The friction coefficient 0.31 is the value between Ti-6Al-4V and 17-4 stainless in air or vacuum. Therefore, the peak displacement of group III & IV, respectively 2.03 mm & 1.79 mm, lie between the values of group I and II.

The ratios between the peak magnitudes of displacements of dynamic and static analysis have been calculated. However, this ratio is not enough to amplify the loading in static analysis, to make the static stress/strain/displacement be over the corresponding dynamic values for each position on the model.

Since it would be a huge job to check the static and dynamic displacement of every location at every time point, conservative DAF is necessary to meet the objectives of this work ( Equation 1, Equation 2, Equation 3).

For the time being, DAF = 1.5 is suggested for group II, III and IV. DAF = 2 is suggested for group I where there are the most “loosen” joints. However, while checking the stress profiles shown in Figure 17, Figure 20 and Figure 23, the suggested DAF = 1.5 have still space to be raised up, since not all locations on the model have higher stress in amplified static analysis than those in dynamic analysis.

If a general DAF is to be proposed, it shall lie between 1.5 and 2.

As a bridge between static and dynamic analysis, a clearer goal of DAF shall be defined: Decisions shall be made that, to which specific goal shall the DAF be applied: Shall the strain / stress/ displacement in the amplified static analysis, of all locations on the components, at all time steps, be over the corresponding values of dynamic analysis? Or only certain values (strain / stress/ displacement) of certain locations of interest, and only at certain time step are to be concerned.

In the future work, moments due to the unevenly distributed EM loadings shall be included in the evaluation of the motion of divertor.

More new results of EM loading shall be applied to the 3D model, and decisions shall be made to determine the designed fixation for closer results to reality.

## 6. Conclusion

Following the presented results and the discussion above, several conclusions have been drawn:

1. The analytical solution of DAF is not applicable for the EM loading acting on divertor, which are usually impact or one-cycle loading. Only initial displacement response of divertor is concerned instead of steady state response.
2. Friction, damping and preload have marginal effect on the calculated eigen-frequencies of divertor.
3. Loosen fixation leads to higher DAF, and vice versa.
4. In order to make corresponding stress / strain / displacement in static analysis be over the values in dynamic analysis, the loading in static analysis shall be amplified by a DAF, which is larger than the ratio between values from dynamic and static FEM analysis.
5. A general DAF is suggested to be between 1.5 and 2 for EM loading on DEMO divertor.

*This work has been carried out within the framework of the EUROfusion Consortium, funded by the European Union via the Euratom Research and Training Programme (Grant Agreement No 101052200 EUROfusion). Views and opinions expressed are however those of the author(s) only and do not necessarily reflect those of the European Union or the European Commission. Neither the European Union nor the European Commission can be held responsible for them.*

## Reference

- [1] G. Mambro, A. Maffucci, G. Mazzone, S. Ventre, F. Villone and J. H. You, „Mechanical impact of electromagnetic transients on the European DEMO divertor. Part 1: Vertical displacement event,“ Fusion Engineering and Design, Bd. 175, Nr. 112999, February 2022.
- [2] J. H. You and et al, „Divertor of the European DEMO: Engineering and technologies for power exhaust,“ Fusion Engineering and Design, Bd. 175, Nr. 113010, February 2022, 113010.
- [3] A. Akay and A. Carcaterra, „Damping Mechanisms,“ in Active and Passive Vibration Control of Structures, CISM International Centre for Mechanical Sciences, 2014.
- [4] „Load\_Specifications\_(LS)\_222OGL\_v6\_1,“ ITER.
- [5] D. Marzullo, „Progress in the pre-conceptual CAD engineering of European DEMO divertor cassette,“ Fusion Eng. Des., Bd. 146, p. 942–945, 2019.
- [6] G. a. Mazzone, „ Eurofusion-DEMO divertor-cassette design and integration.,“ Fusion Eng. Des. , Bd. 157, Nr. 111656, 2020.
- [7] „ABAQUS UNIFIED FEA,“ [Online]. Available: <https://www.3ds.com/products-services/simulia/products/abaqus/>.
- [8] F. Lanzotti, D. Marzullo, V. Imbriani, G. Mazzone, J. H. You and G. D. Gironimo, „Requirements Management in Master Model development: a case study in Fusion Engineering,“ in Int. Joint Conf. on Mechanics, Design Engineering and Advanced Manufacturing, 2022.

- [9] "Dynamic Amplification Factor," [Online]. Available: <https://www.sciencedirect.com/topics/engineering/dynamic-amplification-factor>.
- [10] J. Jenson, "Load and Global Response of Ships," in Elsevier Ocean Engineering Series, 2001.
- [11] "Material Property Handbook EUROFER97 / D25.30\_MAT.D08.8\_APPENDIX\_A\_EUROFER97," EUROfusion.
- [12] J. H. You and H. Bolt, „Overall mechanical properties of fiber reinforced metal matrix composites for fusion applications," Journal of Nuclear Materials, Bd. 305, pp. 14-20, 2002.
- [13] D. Marzullo, B. Motyl, E. Vaglio, S. Filippi, V. Imbriani, G. Mazzone and J. H. You, „Experiences of Additive Manufacturing for nuclear fusion applications: the case of the wishbone of the divertor of DEMO project," in Int. Joint Conf. on Mechanics, Design Engineering and Advanced Manufacturing, 2022.
- [14] A. Pai, „Memo on static co-efficient of friction between similar Stainless Steel 304/304L materials for Cryostat support application," ITER, 2018.
- [15] G. Gironimo, D. Carfora, G. Esposito, A. Lanzotti, D. Marzullo and M. Siuko, „Concept design of the DEMO divertor cassette-to-vacuum vessel locking system adopting a systems engineering approach," Fusion Engineering and Design, Bd. 94, pp. 72-81, 2015.